Pharm Res
DOI 10.1007/s11095-012-0829-y

RESEARCH PAPER

Modeling the Yew Tree Tubulin and a Comparison of its Interaction with Paclitaxel to Human Tubulin

Jack A. Tuszynski • Travis J. A. Craddock • Jonathan Y. Mane • Khaled Barakat • Chih-Yuan Tseng • Melissa Gajewski • Philip Winter • Laleh Alisaraie • Jordan Patterson • Eric Carpenter • Weiwei Wang • Michael K. Deyholos • Linji Li • Xiao Sun • Yong Zhang • Gane Ka-Shu Wong

Received: 6 March 2012 / Accepted: 5 July 2012

ABSTRACT

Purpose To explore possible ways in which yew tree tubulin is naturally resistant to paclitaxel. While the yew produces a potent cytotoxin, paclitaxel, it is immune to paclitaxel's cytotoxic action.

Methods Tubulin sequence data for plant species were obtained from Alberta 1000 Plants Initiative. Sequences were assembled with Trinity *de novo* assembly program and tubulin identified. Homology modeling using MODELLER software was done to generate structures for yew tubulin. Molecular dynamics simulations and molecular mechanics Poisson–Boltzmann calculations were performed with the Amber package to determine binding affinity of paclitaxel to yew tubulin. ClustalW2 program and PHYLIP package were used to perform phylogenetic analysis on plant tubulin sequences.

Results We specifically analyzed several important regions in tubulin structure: the high-affinity paclitaxel binding site, as well as the intermediate binding site and microtubule nanopores. Our analysis indicates that the high-affinity binding site contains several substitutions compared to human tubulin, all of which reduce the binding energy of paclitaxel.

Conclusions The yew has achieved a significant reduction of paclitaxel's affinity for its tubulin by utilizing several specific residue changes in the binding pocket for paclitaxel.

KEY WORDS chemotherapy · nanopores · paclitaxel · tubulin · yew tree

ABBREVIATIONS

1KP	1000 plants initiative
BLAST	basic local alignment search tool
MD	molecular dynamics
MM-PBSA	molecular mechanics Poisson–Boltzmann surface area
MT	microtubule
NDGA	nordihydroguaiaretic acid
ORF	open reading frames
PDB	protein data bank
PTX	paclitaxel
RMSD	root mean square deviation

INTRODUCTION

Motivation

Natural products have been used by humanity as source of medicinal drugs for decades, common drugs such as

J. A. Tuszynski • J. Y. Mane • C.-Y. Tseng • M. Gajewski • P. Winter • L. Alisaraie
Department of Oncology University of Alberta
Edmonton, Alberta, Canada

J. A. Tuszynski • T. J. A. Craddock • K. Barakat
Department of Physics University of Alberta
Edmonton, Alberta, Canada

T. J. A. Craddock • J. Patterson • W. Wang • G. K.-S. Wong
Department of Medicine University of Alberta
Edmonton, Alberta, Canada

K. Barakat
Department of Engineering Mathematics & Physics
Fayoum University
Fayoum, Egypt

E. Carpenter • M. K. Deyholos • G. K.-S. Wong
Department of Biological Sciences University of Alberta
Edmonton, Alberta, Canada

L. Li • X. Sun • Y. Zhang
Guangdong Provincial Engineer Laboratory of Proteomics
BGI-Shenzhen
Yantian District, Shenzhen,
China

Published online: 26 July 2012

quinine, morphine, and aspirin have all been extracted from natural sources. Since the 1950s many anti-mitotic cancer chemotherapy drugs have been extracted from natural sources (1). The main pitfalls and limitations of today's chemotherapy are high toxicity and serious side effects caused by drugs such as paclitaxel (PTX). Simply put chemotherapy does not distinguish between healthy and cancerous cells, and thus adversely affects many vital functions of the body, especially leading to neuropathy, immune system breakdown and numerous other deleterious side effects. However, tumor cells have an ability to resist the action of chemotherapeutic drugs by rapid adaptation to the changing environmental conditions; using efflux pumps to eject toxic molecules, constantly changing the expression of proteins, and developing mutations allowing them to escape effects of the drug.

The anti-mitotic drugs themselves have been extensively studied over many years; however, the genomes and transcriptomes of the plants from which the drugs have been extracted have been sparsely studied. It is one of the many goals of the 1000 Plants Initiative (1KP) (2), a phylogenetically-guided sequencing of plant transcriptomes from angiosperms to algae, to investigate the tubulin sequences of the source plants of the anti-mitotic agents, and utilize this information to understand how the plant cells are resistant to the toxic anti-mitotic agents produced within the plant. One of the important untapped conceptual tools in the design of cancer chemotherapy agents is the understanding of the genes of the source plants from which many of the existing drugs have been derived. The plant expresses a given toxin as a mechanism of self-defense against various predators. While the toxin is fatal to the predator, it is mostly harmless to the host organism. Curiously, both predator and prey express the target protein for the action of the toxin, but not in an identical manner. If we knew what types of differences exist in the host genes that confer resistance against the toxic effects of these compounds, we should be able to adopt the same strategy *vis a vis* the cancer cells (predator) and normal cells (host). In order to acquire this level of understanding we need to sequence the medicinal plant of origin. In the case discussed in this paper, we study the yew tree, which is the main source of PTX. The information unlocked by this study can aid in the understanding of drug resistance that is a common effect limiting the success of numerous chemotherapy drugs including PTX. The first tubulin sequencing experiments have been performed on two yew tree species, and we report these results and their analysis in the present paper.

J. A. Tuszynski (✉)
Department of Oncology, Division of Experimental Oncology
Cross Cancer Institute, 11560 University Ave.
Edmonton, Alberta T6G 1Z2, Canada
e-mail: jackt@ualberta.ca

G. K.-S. Wong
BGI-Shenzhen
Yantian District
Shenzhen, China

Molecular Action of Paclitaxel

Paclitaxel (PTX), developed by Bristol-Meyer-Squibb (trade name Taxol), is one of the most common and successful cancer chemotherapy drugs. PTX is a plant alkaloid isolated from the bark of the yew tree. PTX binds tubulin molecules assembled into microtubules (MTs) and causes stabilization of MTs, which prevents their disassembly and blocks cell division, resulting eventually in apoptosis (3,4).

Shortening of MTs normally occurs when the GTP nucleotides linking individual dimers become hydrolyzed to GDP, causing dimers to depolymerize from the ends of the MT (5). In the absence of PTX, it has been predicted that the energy stored in longitudinal contacts is greater than that stored in lateral contacts (5). Recent results using hydrogen/deuterium exchange coupled with mass liquid chromatography have demonstrated that increased rigidity in PTX stabilized MTs was distinct from stabilization as a result of GTP-induced polymerization (6). These studies suggest that PTX increases the overall energy associated with polymerization while maintaining the same differential between lateral and longitudinal contacts in the MT lattice. Through structural studies taxanes were shown to bind a unique site within the β subunit of the α/β-tubulin heterodimer (7,8). Unfortunately, neither of the structures has been able to reveal the precise mechanism of MT stabilization by these drugs.

When PTX binds to MTs at its site within the lumen, the dynamic properties of the MTs are altered, leading to the stabilization of tubulin against depolymerization (6). The PTX-induced stabilization of MTs is thought to occur through the strengthening of lateral contacts between adjacent protofilaments (6). This stabilization may be a result of PTX's interaction with the flexible M-loop on β-tubulin, resulting in its repositioning relative to the inter-protofilament contact (7). In the presence of PTX, the M-loop is fixed in a conformation favorable to interaction between adjacent protofilaments (8).

Paclitaxel Binding Site in Human β-Tubulin

The first structure of an $\alpha\beta$-tubulin dimer was solved in complex with the PTX analog, docetaxel (8). This structure was quickly followed by a refined tubulin structure containing PTX itself (7). While the initial structure of docetaxel

had clear density for the central "Taxol ring", much of the rest of the molecule's density was not clear and its position was based on a visual fit to the data. The refined structure of tubulin produced improved resolution of the bound PTX molecule, however, the density of the 2-phenyl and N′ phenyl groups remained low due to a certain degree of mobility in these regions. Through their analysis of PTX binding, the authors identified a number of residues that are involved in its interaction with β-tubulin. First, Val23 makes hydrophobic contacts with both the N′ and 3′ phenyl rings while Asp26 is within hydrogen bonding distance to the nitrogen group in PTX's C13 side chain. Additionally, Leu215, Leu217, His227, and Leu228 make hydrophobic contacts with the 2-phenyl ring, while Ala231 and Ser234 contact the 3′ phenyl group. Although Phe270 does not make direct contact with PTX, it was identified as a key residue within the hydrophobic binding pocket. Several residues within the M-loop were also identified as essential for the taxanes' interactions with tubulin, namely Pro272, Leu273, Thr274 (which contacts the essential oxetane ring) as well as Ser275 and Arg276. Additionally, while Pro358, Arg359, Gly360 and Leu361 do not directly interact with PTX, they form the binding pocket itself.

PTX is a relatively large molecule with four side chains extending from its main multi-ring structure. It is possible that its internal flexibility may contribute to reduced van der Waals overlap during its motion to the binding site. One way of quantifying this flexibility is by comparing the energies of conformers relative to the distances between functional groups. From such an analysis of the structure of the implicitly solvated drug, a change of 1 kcal/mol above the lowest energy state was found to correspond to increasing or decreasing the distance between the C2-benzoyl group, and a second group containing both C3′-phenyl and benzoylamino side-chains, by as much as 3 Å from the minimum of 12 Å; with the same energetic penalty, the narrower dimension between the two close C3′-phenyl and benzoylamino rings may be varied from its minimum energy value of 6.6 Å by about 0.5 Å.

We define the PTX binding site as comprised of the residues that occupy the space within a 6 Å radius of PTX, as it is bound to β-tubulin. By this criterion, the residues 22–26, 172–177, 214–217, 223–235, 270–280 and 357–360 are those that interact with PTX (9). Of these 43 amino acids, only five positions show any difference between each of the human β-tubulin isotypes. The β-tubulin isotypes are highly homologous forms of the β-tubulin subfamily encoded by different genes within an organism, which display differential expression patterns throughout the human body (9). The isotypes considered are labeled βI, βIIa, βIIb, βIII, βIVa, βIVb, βV, βVI, and βVIII (corresponding to the genes *TUBB*, *TUBB2A*, *TUBB2B*, *TUBB3*, *TUBB4A*, *TUBB4B*, *TUBB6*, *TUBB1*, and *TUBB8*, respectively; a tenth isotype, βVII, is now known to be a pseudogene, *TUBB7P*), and it turns out that the PTX binding site differences from the consensus sequence occur only within the βIII and βVI sequences. There is one substitution for βIII in PTX binding site, and five substitutions for βVI; note that βVI also has the lowest overall homology with the other members of the β-tubulin subfamily. However, most of these substitutions are conservative, with the exception of the βVI substitution Ser25Gly. The role of human tubulin isotype differences in PTX binding is discussed in more detail below.

Within βIII tubulin there are four substitutions that occur within 10 Å of the bound PTX molecule in the 1JFF structure. All substitutions are superimposable and they occur at the following residue locations within 5–10 Å from PTX: Pro80Ala, Cys239Ser, Ala373Ser; and within 5 Å from PTX: Ser275Ala. The Ser275Ala mutation within the M-loop could play a role in the longitudinal filament interaction. This residue's side chain is facing away from the PTX binding site and would most likely have no direct influence on binding, but may have an effect on MT stabilization. The replacement of Ser275 by alanine in βIII eliminates the γ-oxygen of Ser275. We also focused on the fluctuation of the two atoms that close the binding site (the NH_2 of the guanidinium group of Arg276 and the Nε of the imidazole group of His227). The values for βIII seem to be constant. The substitution of an alanine for a serine adjacent to an arginine, which appears to provide significant steric restrictions in PTX binding kinetics, potentially affects the binding kinetics in the βIII isotype.

Tubulin βVI is more interesting, as there are five differences that occur within 5 Å of the bound PTX molecule, four of which occur within those residues identified by Löwe *et al.* (7) as being critical for PTX binding. These differences are: Val23Met, Asp26Glu, Ala231Leu, Ser275Ala, and Arg276Glu. There is a significant change in the volume of the binding pocket that interacts with the phenyl ring that becomes changed in docetaxel. Reduction of the size of this functional group may increase binding of PTX to this class of β-tubulin. This could involve replacement of the NHCOPh group (bound to C3′) with a methyl group. Note that these substitutions in βVI tubulin do not affect the 3′ phenyl binding pocket. The substitution Val23Met is highly conservative and would not change the hydrophobic interaction with the N′ and 3′ phenyl rings. Due to the increased length of the glutamic acid side chain, the substitution Asp26Glu may have an effect on its ability to form a hydrogen bond with the nitrogen within the C13 side chain of PTX. This substitution may also result in a significant difference to the volume within the portion of the binding pocket that interacts with the PTX 4′ phenyl ring.

Reduction of the size of this functional group, such as in docetaxel, may increase binding of taxanes to βVI tubulin. This difference could also be exploited by the replacement of PTX's C3′ NHCOPh with a methyl group. Ser275Ala is found within the M-loop, but the side chain points away from the PTX-binding site. Finally, within βVI Arg276Gln imparts a slightly increased negative nature to this area and may introduce an increased repulsion between the C7 and C9 oxygen atoms in PTX, resulting in a decrease in binding affinity. In particular Arg276 appears to play a crucial role in PTX binding. It can be observed that the Arg276 side-chain forms a "latch" that could stabilize PTX in its binding pocket in β-tubulin. Since it sticks out and is around PTX and very nearly in contact with His227, it would seem to hold PTX in place and would prevent it from binding. However, the arginine side-chain is quite flexible and can be expected to move out of the way to allow PTX to bind and unbind. Our models have demonstrated that the PTX site exhibits thermal fluctuations that differ among the various isotypes (9).

MATERIALS AND METHODS

Sequence Assembly

Tubulin protein sequences were assembled from the 1KP (2) transcriptome sequence data using the following method. Sequence read data files in FASTQ format were downloaded from the 1KP data-server for seven plant species (Table I). There were two samples for yew tree species: the WWSS (*Taxus baccata* mature leaves and small woody branch) and ZYAX (*Taxus cuspidata* branch apex including needles) samples. The read files were trimmed to remove low quality reads, using a quality threshold of Q20. The reads were assembled using the Trinity assembly software (10). A minimum contig size of 600 nucleotides was used. Assembled sequences matching α-, β- and γ-tubulin were selected using Basic Local Alignment Search Tool (BLAST) (11) and a set of reference tubulin sequences. An e-value threshold of 10^{-4} or below was used to avoid assigning a sequence to the wrong tubulin class. The reference sequences used for BLAST were *Arabidopsis thaliana* mRNA sequences from GenBank (12). The sequence accession codes of the reference sequences for α-tubulin were: NM_105148.3, NM_103889.3, NM_121982.3, NM_100360.3, NM_121983.3, NM_117582.3, and NM_179057.1 The sequence accession codes for β-tubulin were: NM_106228.2, NM_125664.3, NM_125665.3, NM_123801.1, NM_101856.2, NM_121263.3, NM_128508.2, NM_122291.3, NM_001203444.1, and NM_118207.2. The sequence accession codes for γ-tubulin were: NM_116030.1, U02069.1, and U03990.1 Open reading frames (ORFs) were identified and the mRNA sequences translated to protein using the EMBOSS tools (13). Non-unique protein sequences were merged. Protein sequences with a length of less than 360 amino acids, or with large insertions, were discarded.

Homology Modeling

Taxus baccata α-tubulin (WWSSA1, WWSSA2) and β-tubulin (WWSSB1, WWSSB2) sequences, obtained from the 1KP (2) data, were respectively aligned with human α-tubulin (P68366) and β-tubulin (P07437) sequences (corresponding to the genes *TUBA4A* and *TUBB* respectively), as obtained from the UniProt database (14) using EMBOSS software (13). The human tubulin genes *TUBA4A* and *TUBB* were chosen as they tend to be the most highly expressed tubulin isotypes in human tissue (15). The EMBOSS Needle tool uses the sequence alignment technique of Needleman and Wunsch (13) to read two protein input sequences and write their optimal global sequence alignment to file. This procedure used the default settings (BLOSUM62 matrix, open gap penalty=10, extend gap penalty=0.5).

The coordinates of missing residues from the PDB (16) crystal structure of bovine brain tubulin 1JFF (7) were obtained from the 1TUB (8) structure of tubulin after root mean square derivation (RMSD) alignment of the two structures. Using the LEAP module of AMBER 9 (17) with the AMBER99SB force field (18) this repaired 1JFF dimer was solvated in a 25 Å box of TIP3P water and 107 atoms of Na^+ and Cl^- each to bring salt concentration to 0.1 M, then neutralized via the inclusion of an additional 35 Na^+ atoms.

Table I List of Alberta 1000 Plants Initiative (1KP) Samples Selected for Study

Species	Common name	1KP sample code(s)	Tubulin-binding compound(s)
Taxus baccata	English yew	WWSS	Paclitaxel (PTX)
Taxxus cuspidata	Japanese yew	ZYAX	Paclitaxel (PTX)
Catharanthus roseus	Madgascar periwinkle	UOYN	Vinblastine, vincristine
Colchicum autumnale	Autumn crocus	NHIX, OVRB, SFCT	Colchicine
Gloriosa superba	Gloriosa lily	GDKK	Colchicine
Larrea tridentata	Creosote bush	UDUT	Nordihydroguaiaretic acid (NDGA)
Podophyllum peltatum	Mayapple	WFBF	Podophyllotoxin

The system was then energy minimized with periodic boundaries using a conjugate gradient and line search algorithm with PME summation over 40,000 minimization steps using NAMD software (19,20) with these parameters: timestep=2 fs, 1–4 scaling=0.833, cutoff=12.0 Å, switching distance=10 Å, and pairlist distance=13.5 Å.

Using this dimer, MT type B lattice nanopore structures (21) consisting of two protofilaments and two dimers in length (i.e. four dimers overall), were built with PYMOL 0.99rc6 (22) using the MT geometry described in Li *et al.* (23). This minimized repaired 1JFF structure was used as a template for building homology models in MODELLER 9.10 (24) with default parameters. MODELLER 9.10 (24) performs sequence alignment as well as a conjugate gradient optimization followed by molecular dynamics (MD) with simulated annealing to further refine the homology structure. Three different pairs of α/β target sequences were aligned to the template: P68366/P07437, WWSSA1/WWSSB1, and WWSSA2/WWSSB2. Five dimer models were generated for each target sequence. Final dimer models were chosen based on GA431, DOPE and molpdf scores, as well as the lowest RMSD alignment with the template structure. The final dimer models were run through PROCHECK (25) to check the stereochemical quality of the protein structures. Using PYMOL 0.99rc6 (22) the final dimer models for each sequence were built into MT type B lattice structures of two protofilaments two dimers long, based on previously determined MT geometry (23,26).

Molecular Dynamics Simulations

The binding mode for PTX for each protein structure was based on the human tubulin models. These tubulin/PTX structures were used as starting configurations for the subsequent MD simulations. For each system, the AMBER99SB force field (18) was used for protein parameterization. As the parameters for PTX are not included in the standard AMBER99SB parameters, we decided to use the generalized AMBER force field (GAFF) for PTX parameterization (27). GAFF is very similar to and compatible with the traditional AMBER force fields for many reasons. It employs a simple harmonic function form for bonds and angles. GAFF also uses the same van der Waals parameters that are used by the traditional AMBER force fields. All the parameters for bonds and angles were trained using the force field parameters in the traditional AMBER force fields. As was recommended by AMBER developers, we used the AM1-BCC method to calculate the atomic charges for PTX. This method is very efficient and was parameterized to reproduce HF/6-31G* RESP charges.

Protonation states of all ionizable residues were calculated using the program PDB2PQR (28,29). To mimic the physiological conditions in cells, all simulations were performed at 310 K and pH 7 using the NAMD program (19,20). Following parameterization, the tubulin/PTX complexes were immersed in the center of a cube of TIP3P water molecules. The cube dimensions were chosen to provide at least a 15 Å buffer of water molecules around each system. Chloride or sodium counter-ions were added to neutralize the total charge of the complexes by replacing water molecules having the highest electrostatic energies on their oxygen atoms. The fully solvated systems were then minimized and subsequently heated to the simulation temperature with heavy restraints placed on all backbone atoms. Following heating, the systems were equilibrated using periodic boundary conditions for 100 ps and energy restraints reduced to zero in successive steps of the MD simulation. The simulations were then continued for 2 ns during which atomic coordinates were saved to the trajectory every 2 ps for subsequent binding energy analysis.

Binding Energy Calculations

This study utilized the molecular mechanics Poisson–Boltzmann surface area (MM-PBSA) technique to rank PTX binding to the different tubulin structures (30). This method combines molecular mechanics with continuum solvation models. The total free energy is estimated as the sum of average molecular mechanical gas-phase energies (E_{MM}), solvation free energies (G_{solv}), and entropy contributions ($-TS_{\mathrm{solute}}$) of the binding reaction:

$$G = E_{MM} + G_{\mathrm{solv}} - TS_{\mathrm{solute}}. \tag{1}$$

The molecular mechanical (E_{MM}) energy of each snapshot was calculated using the SANDER module of Amber 10 (31) with all pair-wise interactions included using a dielectric constant (ε) of 1.0. The solvation free energy (G_{solv}) was estimated as the sum of electrostatic solvation free energy, calculated by the finite-difference solution of the Poisson–Boltzmann equation in the Adaptive Poisson–Boltzmann Solver (APBS) (32) and non-polar solvation free energy, calculated from the solvent-accessible surface area (SASA) algorithm. Applying the thermodynamic cycle for each protein-PTX complex, the binding free energy was approximated by:

$$\Delta G^{\circ} = \Delta G_{\mathrm{gas}}^{\mathrm{tubulin-PTX}} + \Delta G_{\mathrm{solv}}^{\mathrm{tubulin-PTX}} - \left\{\Delta G_{\mathrm{solv}}^{\mathrm{PTX}} + \Delta G_{\mathrm{solv}}^{\mathrm{tubulin}}\right\}. \tag{2}$$

Here, $\Delta G_{\mathrm{gas}}^{\mathrm{tubulin-PTX}}$ represents the free energy per mole for the non-covalent association of the ligand-protein complex in vacuum (gas phase) at a representative temperature, while ($-\Delta G_{\mathrm{solv}}$) stands for the work required to transfer a molecule from its solution conformation to the same conformation in

vacuum (assuming that the binding conformation of the PTX-protein complex is the same in solution and in vacuum).

Phylogenetic Analysis

To perform the phylogenetic analysis, we first applied ClustalW2 to perform multiple sequence alignment (33). Because the Jones–Taylor–Thornton model considers much larger protein sequence samples than Dayhoff PAM model, it provides better assessment in the probability changes from any amino acid to any other (34). Therefore, it was then utilized to evaluate the similarity of two sequences based on the alignment result obtained previously. Finally, the neighbor-joining method was used to cluster sequences using the similarity matrix generated previously (35). The algorithms were implemented in the PHYLIP package (36). The website iTOL was used to visualize the clustering results (37,38).

RESULTS

Yew Tree Tubulin Sequences

Tubulin sequences were assembled for a selected set of samples from the 1KP (2) project data. Samples were selected because the plant species is known to produce a tubulin-binding compound, or in the same genus or family. Also included was any species in the same genus (or in some cases in the same family). Table I lists the selected samples. The two yew tree species sequenced were *Taxus baccata* (European yew) and *Taxus cuspidata* (Japanese yew). Unfortunately, sequence data for *Taxus brevifolia*, the most well-known source of paclitaxel, was not available from the 1KP data. The chemical precursors of PTX can be derived from the leaves of *Taxus baccata*—which is a more renewable source than the bark of the *Taxus brevifolia*—and the sample of *Taxus baccata* sequenced included mature leaves. Therefore the analysis focused on the *Taxus baccata* tubulin sequences.

In order to compare the amino acid sequences of human tubulin with those obtained for the yew tree, pairwise sequence alignment was performed between human α- and β-tubulin isotypes *TUBA4A* and *TUBB*, and *Taxus baccata* tubulin isotypes WWSSA1, WWSSA2, WWSSB1, and WWSSB2. Therefore, we used the EMBOSS tools to compare these sequences directly. The sequence identity and similarity values are listed in Table II. Sequence identities were found to be greater than 80%, and sequence similarities were found to be greater than 90% for all comparisons except for WWSSB2. This was due to WWSSB2 being only 377 amino acids long, meaning a large portion of the C-terminal region is missing compared to human beta isotypes. The results for the sequence comparison are summarized in Figs. 1 and 2 and Table II.

Table II Sequence Comparison Between Human and *Taxus baccata* (European Yew) Tubulin Protein Sequences

	Identity	Similarity
α-Tubulin		
WWSSA1	377/450 (83.8%)	425/450 (94.4%)
WWSSA2	376/451 (83.4%)	424/451 (94.0%)
β-Tubulin		
WWSSB1	370/451 (82.0%)	412/451 (91.4%)
WWSSB2	312/444 (70.3%)	350/444 (78.8%)

The yew tree α-tubulin sequences (WWSSA1 and WWSSA2) and the β-tubulin sequences (WWSSB1 and WWSSB2) were obtained from the Alberta 1000 plants initiative (1KP) data (2). The human α-tubulin (P68366) and βI tubulin (P07437) sequences (corresponding to the genes *TUBA4A* and *TUBB* respectively), were obtained from the UniProt database (14). The sequences were aligned and with clustalW2 (33)

Yew Tree Tubulin Homology Models

Approximately 65% of the observed differences in both of the *Taxus baccata* sequences are located on the surface of β-tubulin. Interestingly, approximately 95% of these surface substitutions are found on the luminal face of β-tubulin when it is found in a MT configuration, which is the area where PTX binds on a MT surface.

Aside from variation in the C-terminal tail region (the region after position 430) between all human and *Taxus baccata* tubulin sequences, a number of amino acid variations were found in the β-tubulin sequences: the H1 helix (Ile24Val, Ser25Cys, Asp26Glu, Asp26Gly), the H6-H7 loop (Arg216Lys), the H7 helix (Val229Ile, Gly231Ala, Glu234Ser, Cys235Gly), the M loop (Pro268Val, Gln280Asn, Gln280Val), the S9-S10 loop (Arg359Trp, Arg359Lys, Gly360Glu, Leu361Met, Lys362Ser, Ala364Ser, Val365Ser), all of which play a role in PTX binding and action. The majority of these changes were found in the S9-S10 loop. Other variations also occur, but have yet to be characterized in relation to tubulin polymerization dynamics.

The PROCHECK (25) results of all the homology models found more than 89% of the residues in the generated structures were in the most favored positions indicating that reliable quality homology models were built for human *TUBA4A/TUBB* tubulin dimers, as well as the four combinations available for the *Taxus baccata* isotypes. However, due to the shortened length of the WWSSB2 sequence, models containing WWSSB2 are not considered to be reliable.

The homology models for yew tubulin were placed in MT geometry, in order to examine changes in the nanopore structure (21) with the intention of finding out if the yew tree tubulin forms MTs that offer reduced access for PTX molecules to their binding sites via constricted nanopores

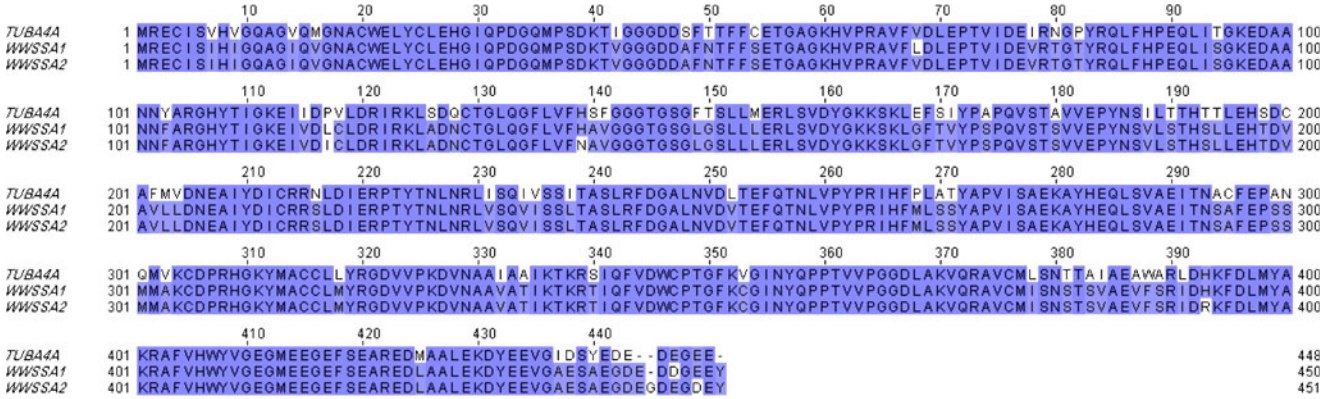

Fig. 1 The sequence alignment of human α-tubulin with yew tree α-tubulin. The human α-tubulin P68366 (gene *TUBA4A*) was obtained from UniProt database (14). The yew tree α-tubulin sequences WWSSA1 and WWSSA2 were obtained from the Alberta 1000 Plants Initiative (1KP) data (2). The sequence alignment was performed with ClustalW2 program (33). Identical residues are shown with a dark blue background. Conservative substitutions are shown with a light blue background. Non-conservative substitutions are shown with a white background.

(Figs. 3, 4). Several residues within 15 Å of the approximate pore centers were found to vary between human and *Taxus baccata* sequences. Modified residues within 15 Å of the nanopore center for nanopore type 1 are α-tubulin Asn216Ser, and β-tubulin Ser126Asn, Ile163Met, Thr285Ser, Asp288Glu, Arg320Lys, Met323Thr, and Lys362Ser. Modified residues within 15 Å of the nanopore center for nanopore type 2 are β-tubulin Ser26Cys, Val113Ile, Ser115Ala, Ser115Gly, Arg216Lys, and Thr221Ser. Among these, a select few belong to the PTX-binding pocket (β-tubulin Lys362, Arg216, and Thr221). However, the overall size and shape of the nanopores was found to be comparable between all models.

Paclitaxel Binding Energy Comparison

Six sequence differences in the PTX binding site region were observed in yew tree WWSSB1 sequence (the shorter WWSSB2 sequence was ignored). The differences are: Ile24Val, Ser25Cys, Asp26Glu, Val229Ile, Gln280Asn, Arg359Trp. For each of these six differences, a protein structure model based on human tubulin β-tubulin with a single residue mutation was generated; and also generated was a protein structure combining all six mutations simultaneously.

The computed relative binding free energies of PTX in each of the protein models is summarized in Table III. As described in the Methods section, binding energies were estimated using the MM-PBSA approach by evaluating the molecular mechanics and solvation energies on the MD trajectory. This approach provided the minimal requirements to incorporate the flexibility of the binding site in evaluating the binding affinity of PTX to all used protein structures. In all cases the truncated model of the tubulin was used, i.e. the C-terminal tail was removed since it is distant from the final binding site of PTX. The root

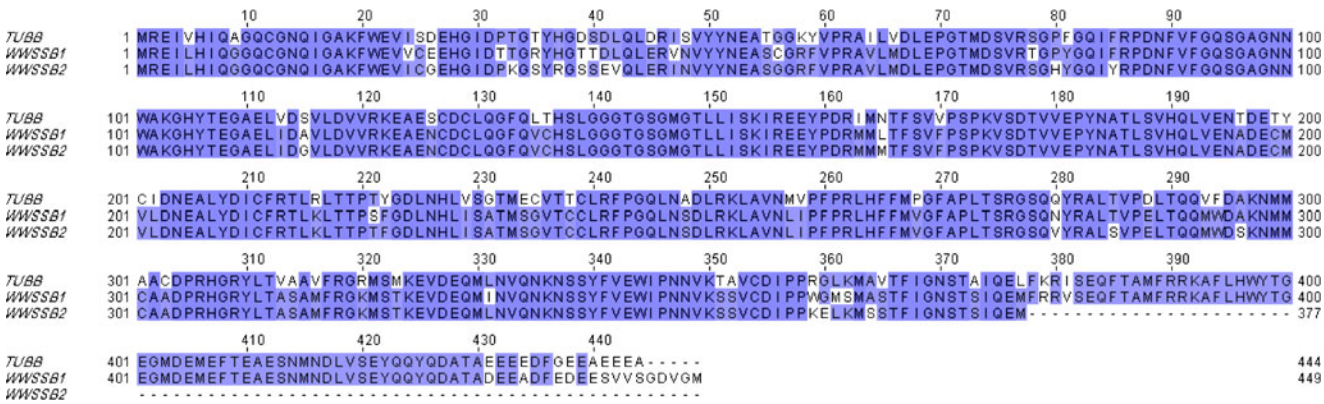

Fig. 2 The sequence alignment of human βI tubulin with yew tree β-tubulin sequences. The human βI tubulin P07437 (gene *TUBB*) was obtained from UniProt database (14). The yew tree β-tubulin sequences WWSSB1 and WWSSB2 were obtained from the Alberta 1000 Plants Initiative (1KP) data (2). The sequence alignment was performed with ClustalW2 program (33). Identical residues are shown with a dark blue background. Conservative substitutions are shown with a light blue background. Non-conservative substitutions are shown with a white background.

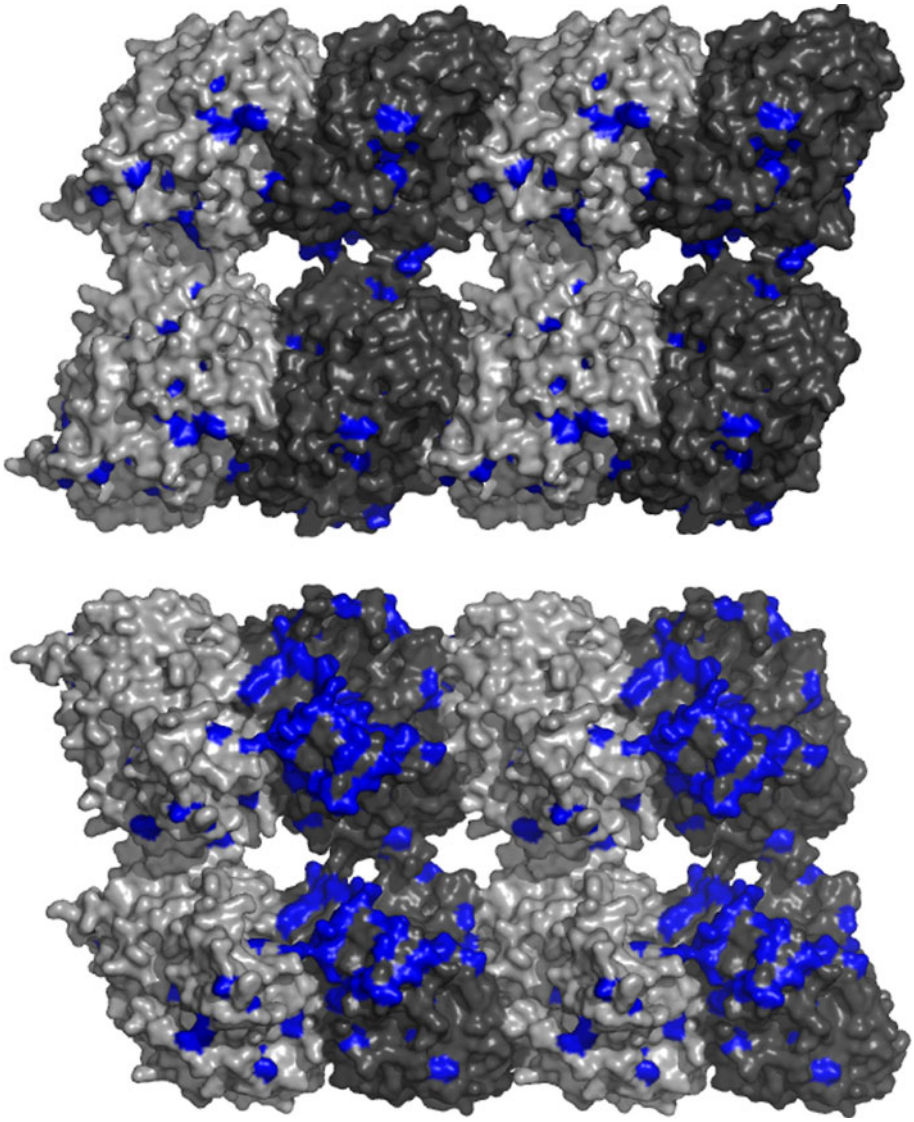

Fig. 3 Short fragments of microtubules illustrating human *TUBA4A/TUBB* nanopores. α-tubulin subunits are light grey and β-tubulin subunits are dark grey; dissimilar residues with one or more *Taxus baccata* tubulin sequences are highlighted in blue. The upper frame shows the microtubule fragment from the outside looking inwards. The lower frame shows the microtubule fragment from in the inside looking outwards. Both fragments are oriented so that the plus end of the microtubule is on the right side of the image. The leftmost and rightmost pores are nanopores of type 1. The center pores are nanopores of type 2.

mean square deviations (RMSD) from the initial minimized structures for three of the studied systems are plotted in Fig. 5. RMSD analysis are given for the both the protein and the PTX ligand. Although the atomic fluctuations of the protein are higher than that of PTX, the three systems reached equilibrium in almost the first 0.5 ns indicating that

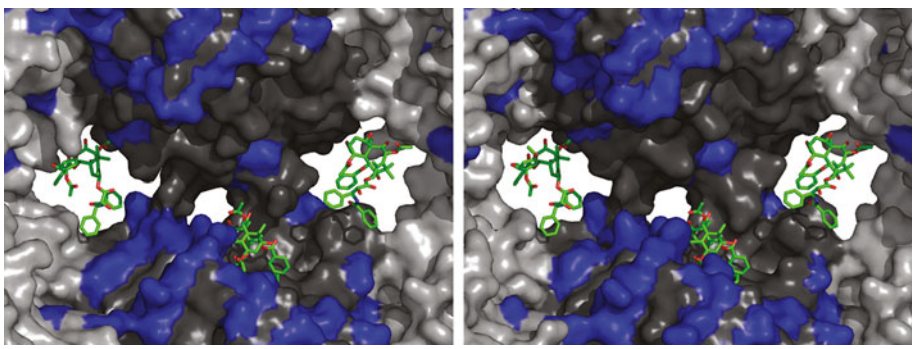

Fig. 4 Human *TUBA4A/TUBB* nanopores (left) and *Taxus baccata* WWSSA1/WWSSB1 nanopores (right). α-tubulin subunits are light grey and β-tubulin subunits are dark grey; dissimilar residues with one or more *Taxus baccata* tubulin sequences are highlighted in blue. Nanopore type 1 is on the left and nanopore type 2 on the right. Paclitaxel (PTX) molecules shown at three sites. The paclitaxel in the center of the image is located at the primary PTX binding site.

Table III The Computed Relative Binding Free Energies ($\Delta\Delta G$) in kcal/mol of Paclitaxel with the Models for Six Single-Residue Mutant Tubulin Protein Structures and a Protein Structure with All Six Mutations Simultaneously

Structure	$\Delta\Delta G$ (kcal/mol)
Ile24Val	+2
Ser25Cys	+1
Asp26Glu	+4
Val229Ile	+9
Gln280Asn	+2
Arg359Trp	+11
All 6 mutations	+8

Binding energies were calculated relative to that of a human-paclitaxel system using human β-tubulin P07437 (βI tubulin, *TUBB* gene), obtained from the UniProt database (14). The binding energies were calculated using the molecular mechanics Poisson-Boltzmann surface area (MM-PBSA) approach by evaluating the molecular mechanics and solvation energies on the molecular dynamics (MD) trajectory (30). Standard errors are ±2 kcal/mol

the 2 ns simulations was adequate for performing the binding energy analysis.

All binding energy calculations were performed on βI tubulin monomer only. Based on the calculations of the binding free energies of PTX on different models of the human βI-tubulin, mutations in positions 25, 229, and 280, i.e. Ser25Cys, Val229Ile, and Gln280Asn, respectively, showed decreased binding of PTX to some degree. Of particular significance appear to be mutations Gln280Asn and Val229Ile, which cause major reduction in the binding free energy. Mutating the PTX binding site simultaneously to the yew tree sequence at positions 24, 25, 26, 229, 280, and 359 with residues Val, Cys, Glu, Ile, Asn and Trp, respectively, is therefore predicted to have significant effects on the binding of PTX.

Phylogenetic Analysis of the Plant Tubulin Sequences

Phylogenetic analysis allows one to quantitatively infer the phylogeny of species of interest (Table I) based on either nucleotide or amino acid sequence information. It assists in inferring common features and evolutionary path across all the species. Since our goal here is not to infer evolutionary path of these species, we focus on applying phylogenetic analysis to infer their relationship and to provide more insight to understand the properties of anticancer agents extracted from them.

The phylogenetic tree of 36 plant tubulin sequences is shown in Fig. 6. Note that since our goal here is not to infer evolutionary path, the tree is only to demonstrate the similarity among these sequences. Namely, the root in top left has no evolutionary meaning. It is not surprising that the phylogenetic tree possesses three large branches, according to the main tubulin subfamilies: α-tubulin, β-tubulin and γ-tubulin. Furthermore, the branch lengths between all α- and β-tubulin are slightly shorter than the lengths either between all α and γ-tubulin or all β- and γ-tubulin.

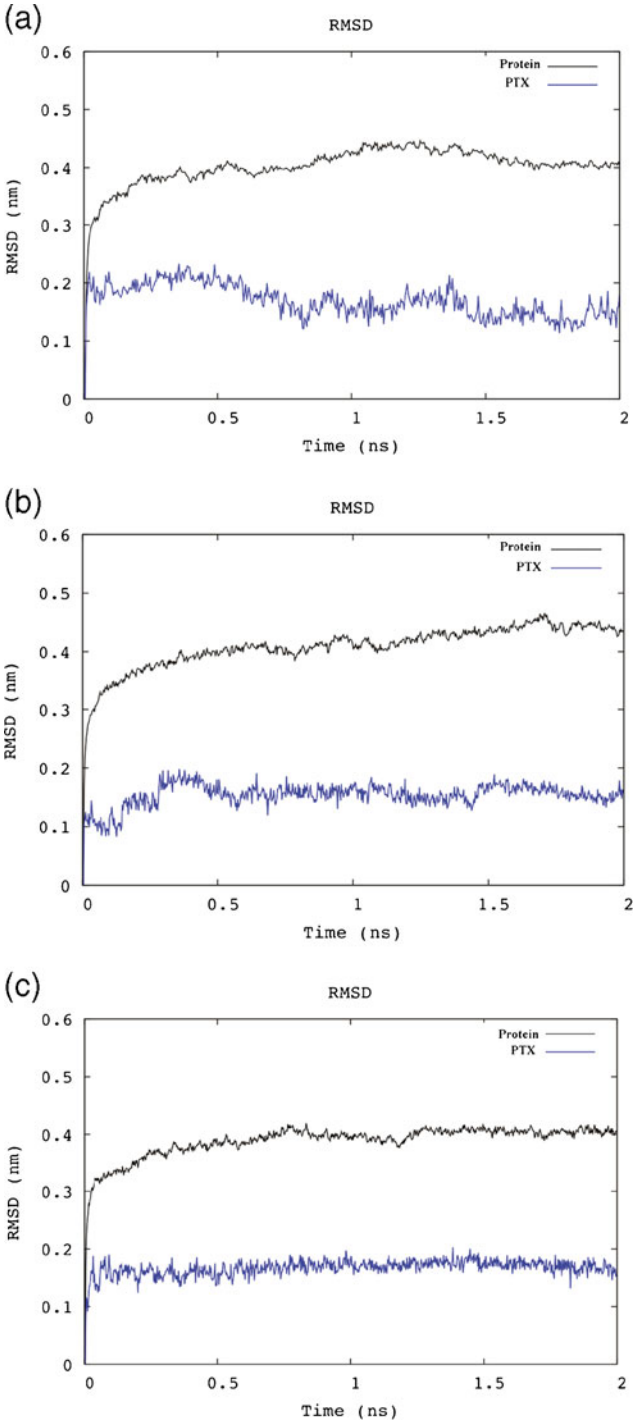

Fig. 5 The root mean square deviations (RMSD) from the initial minimized structures for three of the studied systems: plot (**a**) is human βI tubulin, plot (**b**) is the Ile24Val mutant, and plot (**c**) is the Asp26Glu mutant. RMSD analyses are shown for the both the protein (black curve) and the paclitaxel (PTX) ligand (blue curve). Although the atomic fluctuations of the protein are higher than that of PTX, the three systems reached equilibrium in almost the first 0.5 ns, indicating that the 2 ns simulation period was adequate for performing the binding energy analysis.

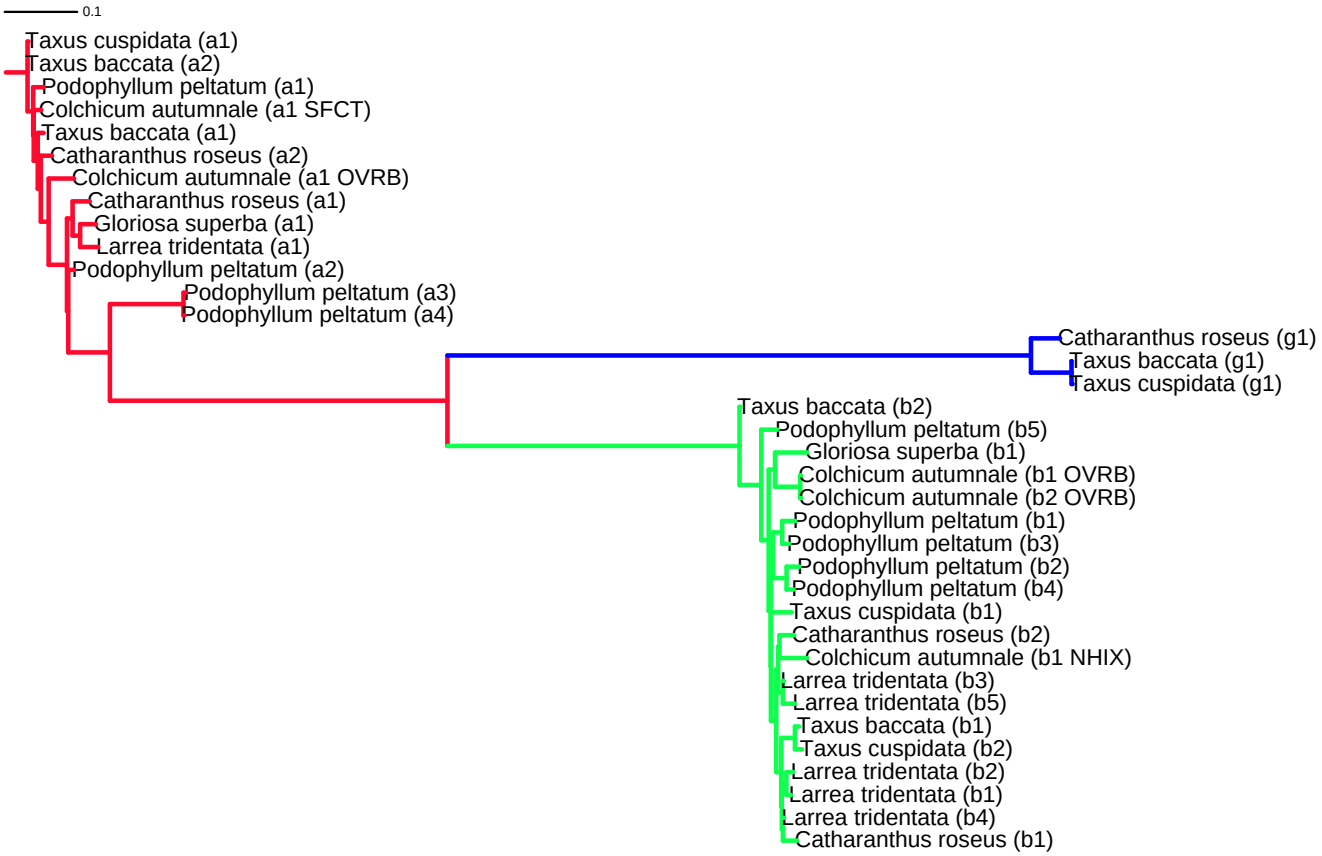

Fig. 6 Phylogenetic tree of tubulin sequences extracted for selected species from the Alberta 1000 Plants Initiative (1KP) data (2). The label inside the round brackets following the species name labels the sequence, with "a" for α-tubulin, "b" for β-tubulin and "g" for γ-tubulin; note that the isotype numbers are assigned arbitrarily. In cases where there were multiple samples for a plant species, the sample code is also given to differentiate the sequences. α-Tubulin sequences are shown with red branches, β-tubulin sequences are shown with green branches (green), and γ-tubulin sequences are shown with blue branches. The branch lengths are related to the relative sequence differences, with shorter lengths indicating sequences that are more similar.

Regarding the PTX, the phylogenetic analysis provides additional information of tubulin sequences from yew trees. In the α-tubulin branch, it can be observed that the branch length between isotype a1 and isotype a2 of α-tubulin from *Taxus cuspidata* and *Taxus baccata* respectively is shorter than the one between isotype a1 and isotype a2 from *Taxus baccata*. Specifically, based on the multiple alignments of α-tubulin isotypes from these two species, the sequences of α-tubulin isotype a1 and isotype a2 from *Taxus cuspidata* and *Taxus baccata* are identical. The α-tubulin isotype a1 from *Taxus baccata* has Ile120Leu, Asn139His, Arg393His, Glu447Asp, and Asp449Glu mutations, and a Gly451 deletion, compared to isotype a2. The next most similar sequence is isotype a1 from *Taxus baccata*.

In the β-tubulin branch, the sequence alignment shows seven mutations Ile6Val, Ala17Ser, Thr31His, Thr36His, Thr39Ser, Ile84Val and Ile368Val in β-tubulin isotype b2 from *Taxus cuspidata* compared to isotype 1 from Taxus baccata. Regarding β-tubulin isotype b2 from *Taxus baccata*, there are 25 mutations compared to isotype b1. There are 27 mutations in β-tubulin isotype b1 from *Taxus cuspidata* compared to isotype b1 from *Taxus baccata*. Thirty mutations are found in β-tubulin isotype b1 and b2 from *Taxus cuspidata*. These results indicate isotype b1 from *Taxus baccata* and isotype b2 from *Taxus cuspidata* have the highest similarity among all β-tubulin isotypes from these two species. Furthermore, the β-tubulin isotypes from other genera that are most closely related to both β-tubulin isotype b2 from *Taxus cuspidata* and isotype b1 from *Taxus baccata* are β-tubulin isotypes b1 and b2 from *Larrea tridentata*. This suggests the compound nordihydroguaiaretic acid (NDGA, also known as masoprocol), which is produced by *Larrea tridentata*, may also share similar binding properties regarding β-tubulin with PTX, as reported by Nakamura *et al.* (39).

DISCUSSION

Paclitaxel Binding and Microtubule Nanopores

With a complex path involved in the binding of PTX, the possibility arises that PTX binding can be influenced by individual residues near, or within, nanopores, and

therefore, that PTX resistance could depend on the precise nature of these residues. In the present work, molecular modeling is used to characterize the putative intermediate binding site within the MT pores and investigate the path taken by PTX from this site to the binding site within the MT lumen.

Several experiments have been designed in order to determine the mechanism by which PTX gains access to its binding site on β-tubulin. While there has been some debate as to the possibility of PTX entering through the open ends of the MT (40), the most recent evidence indicates that PTX must enter the lumen by passing through the MT wall itself. Notably, Ross and Fygensen (41) carried out fluorescence recovery after photobleaching on MTs to observe the diffusion patterns of fluorescently labeled PTX derivatives. They demonstrated a slower fluorescence recovery within thicker MT bundles and that the width of the bleached region changed little with time, indicating lateral diffusion of PTX molecules. Additional evidence for the lateral diffusion of PTX came from work by Buey *et al.* (42) showing that the binding of cyclostreptin, a ligand known to bind at a site near the pore entrance, effectively inhibited PTX binding to the MT lumen. Experimentally determined binding constants were obtained by Díaz *et al.* (43), who observed the diffusion of fluorescently labeled PTX molecules to the binding sites. Their measured rate of binding was much larger than that which was estimated based on steric considerations. Díaz *et al.* concluded that the measured PTX binding was due to an intermediate site that is directly accessible to the bulk solution. Based on molecular modeling and a survey of mutations described in the literature as being associated with acquired resistance to PTX, Díaz *et al.* identified a potential intermediate binding site close to specific residues on the H6-H7 loop that differ in these mutant cell lines (43).

Tubulin is a globular heterodimer. This means that in an MT lattice any lateral arrangement between rows of tubulin molecules will create pores along the interface of their connection (21). One pore (called nanopore type 1) is located in the region where the interdimer α/β interface of one tubulin molecule lies next to the interdimer α/β interface of the adjacent tubulin molecule. A second, apparently smaller, nanopore (called nanopore type 2) arises where the α/β intradimer interface of one tubulin molecule lies next to the α/β intradimer interface of the adjacent tubulin molecule. In addition to these two pores, which fit well in the type B lattice, MTs also contain a "seam", part of a type A lattice; two analogous nanopores, designated type 1 s and type 2 s, would be located along this seam. Here, the bottom and middle protofilaments come together to form the B lattice configuration, typical of most MTs. Only the interface between the top protofilament and the second one down (the MT seam) is commonly comprised of a type A lattice. In the type B lattice, pores of type 1 were observed to be larger than type 2 pores and also appear larger than the two pore types seen at the seams (21).

The type 1 nanopore is the closest to the PTX-binding site and is presumably where PTX most likely enters to access the binding site. We measured the point of closest constriction in this pore; considering heavy atoms only, this corresponds to the distance between the CZ atom of β-tubulin Phe212 and CG2 of α-tubulin Thr130, which ranged from 10.1 to 10.7 Å. Although slightly different values were obtained when examining different isotype models, this was caused by different side chain rotamer states, rather than actual differences between isotypes. For nanopores of type 2, distances of 10.5 to 11.4 Å or 9.6 to 12.7 Å were obtained for measurements taken between β-tubulin Asp128 and each of the two α-tubulin residues Asp218 and Glu220 respectively. For pores along the seam of type 1 s, distances measured between α-tubulin Thr130 and Asp218 of the opposite α-tubulin ranged from 9.7 to 9.9 Å, and for those of type 2s, distances between β-tubulin Phe212 and Asp128 of the opposite β-tubulin varied from 8.0 to 9.9 Å.

We have previously completed automated docking of PTX in each of the two types of pores, clustered at an RMSD of 2 Å (21). These results gave no indication of PTX binding within the type 2 pore. On the other hand, for the type 1 pore the lowest energy cluster was also the largest with 24 elements and a lowest docked energy of −16.31 kcal/mol; moreover, upon examination all results in this cluster show PTX in the same orientation, i.e., this cluster represents a single conformation. The existence of this large cluster gives support to the proposed existence of an intermediate binding site in the pore. Moreover the PTX position and conformation within this cluster is located under the H6/H7 loop in a position similar to that previously predicted by Díaz *et al.* (44). Interestingly, this binding site is physically separated from the luminal binding site by the M-loop, which is normally associated with MT stabilization upon addition of PTX (7). Tubulin isotype substitutions near this site that are known to confer reduced sensitivity or resistance to PTX include Leu215His, Leu215Val, Leu215Ile, and Leu217Arg in the H6/H7 loop, and Thr274Ile and Arg282Asn on the M-loop. These residues are located between the two PTX binding sites; while Leu217 likely stabilizes PTX when bound in the lumen, and Thr274 is also close enough to the luminal binding site to potentially stabilize this binding, residues Leu215 and Arg282 are not part of the luminal binding site and so another explanation for the effects of mutating these residues is needed. These residues could potentially be critical for PTX's binding at the intermediate site within the pore, or in its transition to the observed binding site.

Since PTX most likely traverses the type 1 pore, the residue differences in this pore among β-tubulin isotypes

βI, βIIa, βIIb, βIII, βIVa, and βIVb were examined. Several of the residue substitutions are seen in one cluster at the outer edge of the wide luminal opening of β subunit 2, including residues 33 and 55–57. However, no differences among the human β-tubulin isotypes are observed on the outer rim and only two are observed in the interior of the pore. Specifically a conservative substitution of Thr218Ala on the H6/H7 loop of β-tubulin is observed in βIII MTs, and Ser115Ala is observed in βIVa and βV isotypes. Therefore, among the substitutions observed between β-tubulin isotypes, it seems unlikely that any, except possibly Ser115-Ala, would significantly affect the ability of PTX to access its binding site.

The nanopore comparison between human and yew tree tubulin is depicted in Fig. 3, and close-ups of the nanopores are given in Fig. 4. It is apparent from Fig. 4 that the nanopores between the models are of comparable size, suggesting that pore closure is not the cause of PTX resistance in *Taxus baccata*. While these results suggest that pore closure is not the cause of PTX resistance in *Taxus baccata*, full MD simulations would be required to investigate pore dynamics.

Yew Tree Substitutions and Tubulin Dynamics

It is interesting to note that Mitra and Sept (45) analyzed in great detail the dynamics of PTX binding site in tubulin and stressed the importance of PTX arresting the mobility of selected regions both in the immediate contact area that tubulin makes with the bound PTX molecule, and in distal locations. We have superimposed the changes that occur in yew tree tubulin on the Mitra and Sept diagram of significant regions for tubulin dynamicity, and found the following residue numbers of significance to tubulin dynamics: 9, 39–43, 64, 66, 218, 221, 275, 280, 282. Of these residues, only residues 275 and 280 are identified as located within 6 Å of the bound PTX. Consequently, we expect that the combined effect of all the residue changes in the yew tree may be even greater than our calculations indicate.

Yew Tree Substitutions and Taxane Resistance

Based on an examination of the differences observed at the PTX binding site, it is suggestive that there are a disproportionately large number of substitutions located within the PTX binding site, when compared to the human β-tubulin isotypes (9). More than six different substitutions have been found in the yew tree sequences as compared to only one in all of the common human isotypes (excluding βVI). Importantly, the two specific β-tubulin residue positions, 26 and 231, have been observed to vary in both the yew tree sequences and in mammalian cell lines with a taxane-resistant phenotype (46,47), which suggests that tubulin mutations are an important mechanism for taxane resistance. This observation merits further analysis and potentially experimental testing using site mutagenesis methods.

Cysteine Residue Substitutions

It is interesting that there are a disproportionately large number of cysteine substitutions when compared to the human β-tubulin isotypes (9). There are six positions where the yew tree β-tubulin sequences have cysteine substitutions, namely 25, 56 (only in 60% of the yew tree sequences), 136, 199, 238, and 301. Figure 7 shows the positions where the yew β-tubulin sequences have cysteine substitutions not found in human β-tubulin. Also, residue 239 is a cysteine in all the yew tree sequences but only about 60% of the human sequences. It may be worth investigating if these cysteine substitutions are specific to yew tubulin, or if they are conserved across other plant species.

In Table IV we list critical cysteine residues in human β-tubulin isotypes, and note that residue 239 is particularly important (48). Note that tubulin βIII (and also βV and βVI) lacks Cys239, which reacts with peroxy-nitrite to form a disulfide bond with a cysteine in α-tubulin. This may contribute to the dynamicity of MTs built from this isotype of tubulin.

Paclitaxel and Nordihydroguaiaretic Acid

Studies have shown that both NDGA and PTX can stabilize MTs (39). However, the degree of stabilization from PTX is larger than NDGA. Furthermore, NDGA does not affect [^{3}H]PTX binding to β-tubulin. This suggests NDGA has a different binding site than PTX. Namely, the mechanism of stabilizing MTs by NDGA is likely different from PTX. The phylogenetic analysis provides a sequence level understanding on different effects of PTX and NDGA in stabilizing MT. Specifically, one can attribute it to the 19 substitutions in isotype b1 from *Larrea tridentata*, compared to isotype b1 from *Taxus baccata*. Sequence alignment shows that γ-tubulin from *Taxus cuspidata* and *Taxus baccata* are identical, while the α- and β-tubulin sequences of these two species are slightly different.

CONCLUSIONS

In this paper we have provided an overview of the sequence and structure of yew tree tubulin with respect to paclitaxel binding and made a detailed comparison to human tubulin sequences. Understanding the nature of sequence of differences between plant tubulin and human tubulin can provide valuable insights into potential difficulties of application of PTX, which is produced by yew tree, in cancer patients with specific expressions of or mutations in tubulin isotypes. Yew

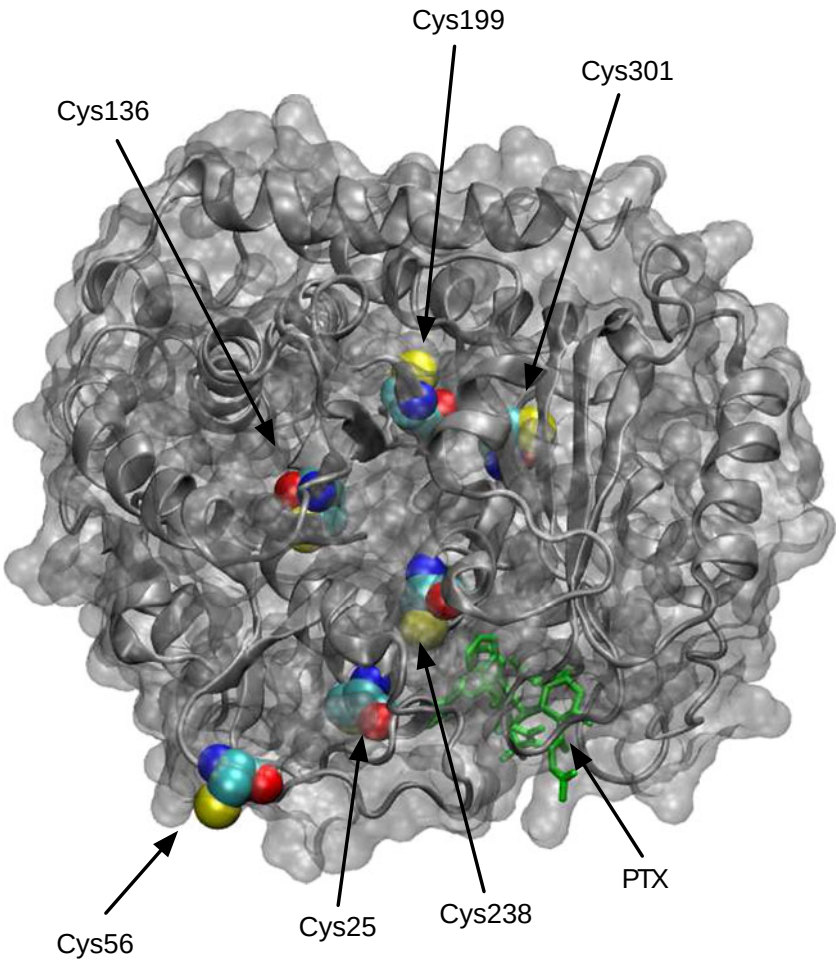

Fig. 7 Positions where the yew tree β-tubulin sequences have cysteine substitutions that are not found in human β-tubulin. The positions are 25, 56 (only cysteine in some yew β-tubulin sequences), 136, 199, 238 and 301. A β-tubulin structure is shown in grey. The cysteine residues are shown as van der Waals spheres. A bound paclitaxel (PTX) molecule is shown in green. Only Cys56 is near the protein surface; the other cysteine substitutions are deeply buried.

tree mutations can provide a guide to seek similarities in patients with drugs resistance, and possibly even predict drug resistance. We have specifically analyzed several important regions in the tubulin structure: the high-affinity binding site, the intermediate binding site and the structure of nanopores, which are implicated in PTX transport into the MT lumen. Our analysis indicates that the high-affinity binding-site contains several amino acid changes compared to human tubulin, all of which reduce the binding energy of PTX and their combination makes binding very weak.

Table IV Critical Cysteines in Human β-tubulin Isotypes (48)

	Position			
Isotype	124	127	129	239
βI	Ala	Cys	Cys	Cys
βIIa	Ser	Cys	Cys	Cys
βIIb	Ser	Cys	Cys	Cys
βIII	Cys	Cys	Cys	Ser
βIVa	Ala	Cys	Cys	Cys
βIVb	Ala	Cys	Cys	Cys
βV	Cys	Cys	Cys	Ser
βVI	Ser	Cys	Cys	Ser

ACKNOWLEDGMENTS AND DISCLOSURES

J.A.T. acknowledges support for this research from the Alberta Cancer Foundation, Alberta Advanced Education and Technology, the Allard Foundation, the Canadian Breast Cancer Foundation, and the National Sciences and Engineering Research Council of Canada (NSERC Canada). T.J.A.C. acknowledges funding support for this research from NSERC Canada. G.K.S.W. acknowledges Alberta Advanced Education and Technology, Genome Alberta, Alberta Innovates Tech Futures iCORE, Musea Ventures, and BGI-Shenzhen for the funding of the Alberta 1000 Plants Initiative.

REFERENCES

1. Cragg GML, Kingston DGI, Newman DJ. Anticancer agents from natural products. 2nd ed. Boca Raton: CRC; 2011.

2. The Alberta 1000 Plants Initiative (Alberta Advanced Education and Technology, Musea Ventures, BGI-Shenzhen, Alberta iCORE, to Wong GKS). Available from: http://www.onekp.com/.
3. Wani MC, Taylor HL, Wall ME, Coggon P, McPhail AT. Plant antitumor agents. VI. The isolation and structure of taxol, a novel antileukemic and antitumor agent from Taxus brevifolia. J Am Chem Soc. 1971;93(9):2325–7.
4. Schiff PB, Horwitz SB. Taxol stabilizes microtubules in mouse fibroblast cells. Proc Natl Acad Sci U S A. 1980;77(3):1561–5.
5. VanBuren V, Odde DJ, Cassimeris L. Estimates of lateral and longitudinal bond energies within the microtubule lattice. Proc Natl Acad Sci U S A. 2002;99(9):6035–40.
6. Xiao H, Verdier-Pinard P, Fernandez-Fuentes N, Burd B, Angeletti R, Fiser A, *et al.* Insights into the mechanism of microtubule stabilization by Taxol. Proc Natl Acad Sci U S A. 2006;103(27):10166–73.
7. Löwe J, Li H, Downing KH, Nogales E. Refined Structure of alpha beta-tubulin at 3.5 A resolution. J Mol Biol. 2001;313(5):1045–57.
8. Nogales E, Wolf SG, Downing KH. Structure of the alpha beta tubulin dimer by electron crystallography. Nature. 1998;391(6663):199–203.
9. Huzil JT, Ludueña RF, Tuszynski J. Comparative modelling of human β tubulin isotypes and implications for drug binding. Nanotechology. 2006;17(4):S90–S100.
10. Grabherr MG, Haas BJ, Yassour M, Levin JZ, Thompson DA, Amit I, *et al.* Full-length transcriptome assembly from RNA-Seq data without a reference genome. Nat Biotechnol. 2011;29:644–52.
11. Altschul SF, Gish W, Miller W, Myers EW, Lipman DJ. Basic local alignment search tool. J Mol Biol. 1990;215(3):403–10.
12. Benson DA, Karsch-Mizrachi I, Clark K, Lipman DJ, Ostell J, Sayers EW. GenBank. Nucleic Acids Res. 2012;40:D48–53.
13. Rice P, Longden I, Bleasby A. EMBOSS: the European Molecular Biology Open Software Suite. Trends Genet. 2000;16(6):276–7.
14. The UniProt Consortium. Reorganizing the protein space at the Universal Protein Resource (UniProt). Nucleic Acids Res. 2012;40:D71–5.
15. Ludueña RF, Banerjee A. The isotypes of tubulin. In: Fojo T, editor. The role of microtubules in cell biology, neurobiology, and oncology. Totowa: Humana; 2008. p. 123–75.
16. Bernstein FC, Koetzle TF, Williams GJ, Meyer Jr EE, Brice MD, Rodgers JR, *et al.* The Protein Data Bank: a computer-based archival file for macromolecular structures. J Mol Biol. 1977;112(3):535–42.
17. Case DA, Darden TA, Cheatham III TE, Simmerling CL, Wang J, Duke RE, *et al.* AMBER 9. San Francisco: University of California; 2006.
18. Hornak V, Abel R, Okur A, Strockbine B, Roitberg A, Simmerling C. Comparison of multiple Amber force fields and development of improved protein backbone parameters. Proteins. 2006;65(3):712–25.
19. Phillips JC, Braun R, Wang W, Gumbart J, Tajkhorshid E, Villa E, *et al.* Scalable molecular dynamics with NAMD. J Comput Chem. 2005;26(16):1781–802.
20. Kalé L, Skeel R, Bhandarkar M, Brunner R, Gursoy A, Krawetz N, *et al.* NAMD2: greater scalability for parallel molecular dynamics. J Comput Phys. 1999;151(1):283–312.
21. Freedman H, Huzil JT, Luchko T, Ludueña RF, Tuszynski JA. Identification and characterization of an intermediate taxol binding site within microtubule nanopores and a mechanism for tubulin isotype binding selectivity. J Chem Inf Model. 2009;49(2):424–36.
22. DeLano W. PyMOL Release 0.99. Palo Alto: DeLano Scientific LLC; 2002.
23. Li H, DeRosier DJ, Nicholson WV, Nogales E, Downing KH. Microtubule structure at 8 A resolution. Strucr. 2002;10:1317–28.
24. Sali A, Blundell TL. Comparative protein modeling by satisfaction of spatial restraints. J Mol Biol. 1993;234(3):779–815.
25. Laskowski RA, MacArthur MW, Moss DS, Thornton JM. PROCHECK: a program to check the stereochemical quality of protein structures. J Appl Cryst. 1993;26(2):283–91.
26. Sept D, Baker NA, McCammon JA. The physical basis of microtubule structure and stability. Protein Sci. 2003;12(10):2257–61.
27. Wang J, Wolf RM, Caldwell JW, Kollman PA, Case DA. Development and testing of a general amber force field. J Comput Chem. 2004;25:1157–74.
28. Dolinsky TJ, Czodrowski P, Li H, Nielsen JE, Jensen JH, Klebe G, *et al.* PDB2PQR: expanding and upgrading automated preparation of biomolecular structures for molecular simulations. Nucleic Acids Res. 2007;35:W522–5.
29. Dolinsky TJ, Nielsen JE, McCammon JA, Baker NA. PDB2PQR: an automated pipeline for the setup, execution, and analysis of Poisson-Boltzmann electrostatics calculations. Nucleic Acids Res. 2004;32:W665–7.
30. Kollman PA, Massova I, Reyes C, Kuhn B, Huo S, Chong L, *et al.* Calculating structures and free energies of complex molecules: combining molecular mechanics and continuum models. Acc Chem Res. 2000;33(12):889–97.
31. Case DA, Darden TA, Cheatham III TE, Simmerling CL, Wang J, Duke RE, *et al.* AMBER 10. San Francisco: University of California; 2008.
32. Baker NA, Sept D, Joseph S, Holst MJ, McCammon JA. Electrostatics of nanosystems: application to microtubules and the ribosome. Proc Natl Acad Sci U S A. 2001;98(18):10037–41.
33. Larkin M, Blackshields G, Brown N, Chenna R, McGettigan P, McWilliam H, *et al.* ClustalW and Clustal X version 2.0. Bioinformatics. 2007;23(21):2947–8.
34. Jones DT, Taylor WR, Thornton JM. The rapid generation of mutation data matrices from protein sequences. Comput Appl Biosci. 1992;8(3):275–82.
35. Saitou N, Nei M. The neighbor-joining method: a new method for reconstructing phylogenetic trees. Mol Biol Evol. 1987;4(4):406–25.
36. Felsenstein J. PHYLIP—phylogeny inference package (version 3.2). Cladistics. 1989;5:164–6.
37. Letunic I, Bork P. Interactive Tree Of Life (iTOL): an online tool for phylogenetic tree display and annotation. Bioinformatics. 2007;23(1):127–8.
38. Letunic I, Bork P. Interactive Tree Of Life v2: online annotation and display of phylogenetic trees made easy. Nucleic Acids Res. 2011;39:W475–8.
39. Nakamura M, Nakazawa J, Usui T, Osada H, Kono Y, Takatsuki A. Nordihydroguaiaretic acid, of a new family of microtubule-stabilizing agents, shows effects differentiated from paclitaxel. Biosci Biotechnol Biochem. 2003;67(1):151–7.
40. Díaz JF, Valpuesta JM, Chacón P, Diakun G, Andreu JM. Changes in microtubule protofilament number induced by Taxol binding to an easily accessible site. Internal microtubule dynamics. J Biol Chem. 1998;273(50):33803–10.
41. Ross JL, Fygenson DK. Mobility of taxol in microtubule bundles. Biophys J. 2003;84(6):3959–67.
42. Buey RM, Calvo E, Barasoain I, Pineda O, Edler MC, Matesanz R, *et al.* Cyclostreptin binds covalently to microtubule pores and lumenal taxoid binding sites. Nat Chem Biol. 2007;3(2):117–25.
43. Díaz JF, Barasoain I, Souto AA, Amat-Guerri F, Andreu JM. Macromolecular accessibility of fluorescent taxoids bound at a paclitaxel binding site in the microtubule surface. J Biol Chem. 2005;280(5):3928–37.

44. Díaz JF, Barasoain I, Andreu JM. Fast kinetics of Taxol binding to microtubules. Effects of solution variables and microtubule-associated proteins. J Biol Chem. 2003;278(10):8407–19.
45. Mitra A, Sept D. Taxol allosterically alters the dynamics of the tubulin dimer and increases the flexibility of microtubules. Biophys J. 2008;95(7):3252–8.
46. Hari M, Loganzo F, Annable T, Tan X, Musto S, Morilla DB, *et al*. Paclitaxel-resistant cells have a mutation in the paclitaxel-binding region of beta-tubulin (Asp26Glu) and less stable microtubules. Mol Cancer Ther. 2006;5(2):270–8.
47. Verrills NM, Flemming CL, Liu M, Ivery MT, Cobon GS, Norris MD, *et al*. Microtubule alterations and mutations induced by desoxyepothilone B: implications for drug-target interactions. Chem Biol. 2003;10(7):597–607.
48. Ludueña RF. Multiple forms of tubulin: different gene products and covalent modifications. Int Rev Cytol. 1998;178:207–75.